# Rapid Maneuvering Control of Pectoral Fin-Actuated Robotic Fish

Maria L. Castaño and Xiaobo Tan

Abstract—The virtues of being maneuverable, efficient, and lifelike have made robotic fish an appealing choice in a wide range of applications. Their agile locomotion can be partially attributed to their bio-inspired propulsion methods. Pectoral fins have in particular become an important form of propulsion for robotic fish, as they play a vital role in achieving agile maneuvering at low swimming speeds. Despite the benefits it offers, pectoral finbased locomotion presents significant challenges in the control of robotic fish. The range constraint of the fin movement can often inhibit the robot from generating thrust in a direction required for maneuvering. The latter could necessitate the fin moving first in a direction opposite to the desired one (which in turn generates unwanted drag) in order to "back up" and create enough room for accelerating. While seeming natural for fish or humans, such fin maneuvers are difficult to engineer with existing control design methods. To overcome these challenges and achieve quick maneuvering control, in this paper, we propose a dual-loop control approach, composed of a backstepping-based controller in the outer loop and a fin movement-planning algorithm in the inner loop. In particular, for the inner loop, we propose a model-predictive planning scheme based on a randomized sampling algorithm that accommodates the fins' constraints and "intelligently" determines the necessary fins' movements to produce a desired thrust despite the fins' current configuration. Simulation results are presented to demonstrate the performance of the proposed scheme via comparison with a nonlinear model predictive controller in rapid velocity maneuvering.

# I. INTRODUCTION

In recent years, bio-inspired underwater robots that propel and maneuver themselves like real fish, often called robotic fish, have emerged as promising platforms for a myriad of applications, such as aquatic environmental monitoring, search and rescue, and robot-animal interactions [1]–[3]. Their efficiency, maneuverability, and stealth are some of the characteristics that have made robotic fish an attractive choice over traditional propeller-driven underwater vehicles [4].

A variety of different fish swimming modes have been explored in the design of robotic fish, including the use of tail (caudal) fin [5], paired pectoral fins [6], a combination of both movements [7], and undulatory motion of the whole body [8]. While caudal fins have proven to be an efficient propulsion mode at higher speeds, pectoral fins provide remarkable maneuvering and efficient propulsion at lower swimming speeds and have thus become a useful actuation mechanism for robotic fish [9].

Pectoral fin motions can generally be classified into three modes based on the axis of rotation: rowing, feathering and flapping, where the axes of rotation are vertical, transverse, and longitudinal, respectively. Rowing motion is classified as a "drag-based" swimming mechanism, where the drag element of fluid dynamics generates the thrust, and it is often regarded as an effective type of motion for achieving a number of in-plane locomotion and maneuvering tasks, such as forward swimming, sideway swimming, and turning [10], [11]. The rowing motion of pectoral fins comprises two sub-movements during the finbeat cycle, namely, a power stroke and a recovery stroke. During the power stroke, the pectoral fin moves backward to produce thrust through induced drag on the pectoral fin surface, while during the recovery stroke, the fin moves toward the front of the body, ideally with minimal loading, to get ready for the next fin-beat cycle.

Although beneficial in maneuvering, utilizing rowing motion for propulsion gives rise to challenges for the control of robotic fish. The challenge lies with the actuation constraints (i.e., angular position, velocity, and acceleration limitations) as well as the mechanism in which the "drag-based" swimming method is used to generate thrust. For example, forward thrust can only be generated during the power stroke; however, when the pectoral fin reaches its maximum angular position, it has to recover in order to be able to generate forward thrust again. During the recovery phase, the fin will actually produce a "negative" thrust, thus opposing the objective of producing forward thrust. While such "backing-up" behavior seems natural to human understanding and is widely used by live fish, it is challenging to incorporate this behavior through systematic, rigorous controller synthesis.

While there is extensive literature available on the design and modeling of pectoral fin-actuated robotic fish [8], [9], [12]-[18], limited work has been reported on the control of these robots. Some of the work in this area has focused on open-loop motion control, i.e., the generation of coordinated movements of the actuation components to produce some fish-like swimming gaits [19]-[21]. In terms of closed-loop control, several authors have proposed sensory-feedback Central Pattern Generators (CPGs) for target tracking or obstacle avoidance control [22], [23]. Similarly, in [24] the authors proposed a control strategy composed of two layers: an upper decision-making layer that used a finite state machine to determine the appropriate swimming gait and a layer that uses a CPG to implement the desired gait. Fuzzy rule-based control laws were proposed in [25] to control fin-beat parameters to drive a robotic fish to perform rendezvous and docking in a three-dimensional workspace. The authors in [18] implemented geometric-control methods for closed-loop depth control of a robotic fish using pectoral fins undergoing feathering motion. All of the aforementioned work utilized cyclic fin actuation for

<sup>\*</sup>This research was supported in part by the National Science Foundation (DGE 1424871, IIS 1715714, IIS 1848945).

 $<sup>^1\</sup>mathrm{Maria}$  Castaño and Xiaobo Tan are with the Department of Electrical and Computer Engineering, Michigan State University, East Lansing, MI 48824, USA. Email: castanom@msu.edu (M.C), xbtan@egr.msu.edu (X.T)

the lead-lag or feathering motion of the fins and treated the finbeat parameters or the phase differences between the fins as the control variables for the fish locomotion control. However, such cyclic fin movement limits precise manipulation of the fin movements and the thrust profile that can be generated, which impedes full exploitation of the maneuverability of pectoral fin-actuated robotic fish. Acyclic thrust or moments could be more instrumental for generating a quick maneuvering response, which can be valuable in scenarios like counteracting disturbances or avoiding fast obstacles.

In this work, we propose a systematic approach to the control of pectoral fins that naturally accommodates the fins' constraints and automatically generates "intelligent" behavior (like fin backing-up when required) to produce acyclic thrust for quick maneuvering. In particular, we consider the velocity tracking problem as an example to illustrate the challenges and propose a dual-loop control structure to drive the velocity tracking error to a neighborhood of the origin. The outer loop of the proposed scheme is composed of a backstepping-based velocity-tracking controller that finds the needed thrust and moment for the robot's velocity to track the desired profile value. The inner loop is composed of a randomized, modelpredictive fin planning algorithm, which determines a feasible sequence for the fins' angular accelerations such that the thrust and moments generated are close to desired values. We utilize a dynamic model based on blade element theory for rigid pectoral fins to design the outer loop controller. Finally, to demonstrate the effectiveness of the proposed scheme, we present simulation results on tracking abruptly changing forward and angular velocities, where the proposed scheme is compared with an alternative approach, in which the inner loop is implemented with a nonlinear model predictive controller (NMPC).

The rest of the paper is organized as follows. We first review the dynamic model of the pectoral fin-actuated robotic fish in Section II. In Section III, we present the proposed control approach in detail. In Section IV, simulation results are discussed. Finally, we provide some concluding remarks in Section V.

# II. DYNAMIC MODEL OF PECTORAL FIN-ACTUATED ROBOTIC FISH

# A. Rigid Body Dynamics

We consider the robot to be a rigid body with rigid pectoral fins that are actuated at the base, and we assume that the robot operates in an inviscid, irrotational, and incompressible fluid within an infinite domain.

As illustrated in Fig. 1(a), we define  $[X,Y,Z]^T$  and  $[\hat{x},\hat{y},\hat{z}]^T$  as the inertial coordinate system and the body-fixed coordinate system, respectively. The velocity of the center of mass in the body-fixed coordinates is expressed as  $V_c = [V_{c_x}, V_{c_y}, V_{c_z}]$ , where  $V_{c_x}$ ,  $V_{c_y}$ , and  $V_{c_z}$  indicate surge, sway, and heave velocities, respectively. The angular velocity expressed in the body-fixed coordinate system is given by  $\omega = [\omega_x, \omega_y, \omega_z]$ , which is composed of roll  $(\omega_x)$ , pitch  $(\omega_y)$ , and yaw  $(\omega_z)$ . We

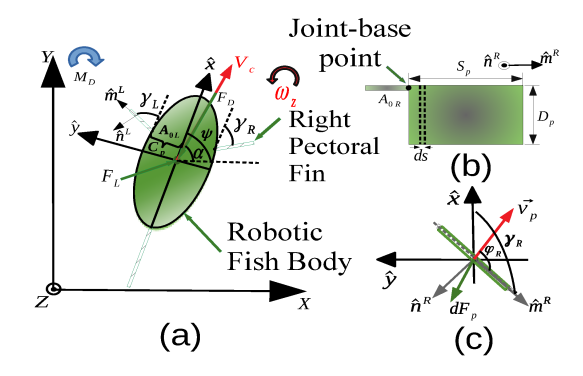


Fig. 1: (a) Top view of the pectoral fin-actuated robotic fish undergoing planar motion, (b) Side view and blade element of the right pectoral fin with its parameters and variables, (c) Top view of the pectoral fin with its associated forces and angles.

let  $\alpha$  denote the angle of attack, formed by the direction of  $V_c$  with respect to the  $\hat{x}$ -axis and is given by  $\alpha = \arctan(\frac{V_{c_y}}{V_{c_x}})$ . Let  $\psi$  denote the heading angle, formed by the  $\hat{x}$ -axis relative to the X-axis,  $C_p$  be the distance between the pectoral fin base and the body's center of mass, and  $A_{0L}$  and  $A_{0R}$  denote the pivot points for the left and right fins, respectively. Finally,  $\gamma_L$  and  $\gamma_R$  represent the angles between the left pectoral fin and the body-fixed  $\hat{x}$ -axis and the right pectoral fin and the body-fixed  $\hat{x}$ -axis, respectively.

We only consider the robot's planar motion, and further assume that the body is symmetric with respect to the  $\hat{x}\hat{z}$ -plane and that the pectoral fins move on the  $\hat{x}\hat{y}$ -plane, such that the system only has three degrees of freedom, surge  $(V_{c_x})$ , sway  $(V_{c_y})$ , and yaw  $(\omega_z)$ . Furthermore, we assume that we can neglect the inertial coupling between yaw, sway and surge motions [26], and arrive at the following equations of planar motion

$$(m_b - m_{a_x})\dot{V}_{c_x} = (m_b - m_{a_y})V_{c_y}\omega_z + f_x$$
 (1)

$$(m_b - m_{a_y})\dot{V}_{c_y} = -(m_b - m_{a_x})V_{c_x}\omega_z + f_y$$
 (2)

$$(J_{bz} - J_{a_z})\dot{\omega}_z = (m_{a_y} - m_{a_x})V_{c_x}V_{c_y} + \tau_z \tag{3}$$

where  $m_b$  is the mass of the body,  $J_{bz}$  is the inertia of the body about the  $\hat{z}$ -axis,  $m_{a_x}$  and  $m_{a_y}$  are the hydrodynamic derivatives that represent the added masses of the robotic fish along the  $\hat{x}$  and  $\hat{y}$  directions, respectively, and  $J_{a_z}$  represents the added inertia effect of the body about the  $\hat{z}$  direction. Finally, the hydrodynamic forces and moment due to the pectoral fin actuation and the interaction of the body itself with the fluid are captured by  $f_x$ ,  $f_y$ , and  $\tau_z$  and are given by

$$f_x = f_{h_x} - F_D \cos(\alpha) + F_L \sin(\alpha) \tag{4}$$

$$f_y = f_{h_y} - F_D \sin(\alpha) - F_L \sin(\alpha) \tag{5}$$

$$\tau_z = \tau_{h_z} + M_D \tag{6}$$

where  $f_{h_x}$ ,  $f_{h_y}$ , and  $\tau_{h_z}$  are the hydrodynamic forces and moment transmitted to the fish body by the right and left pectoral fins, while  $F_D$ ,  $F_L$ , and  $M_D$  are the body drag, lift, and moment, respectively.

### B. Drag and Lift on the Robot Body

The lift force  $F_L$ , drag force  $F_D$ , and drag moment  $M_D$ acting on the robotic fish can be captured by ([18], [27])

$$F_D = \frac{1}{2}\rho |V_c|^2 S_A C_D \tag{7}$$

$$F_L = \frac{1}{2}\rho |V_c|^2 S_A C_L \alpha \tag{8}$$

$$M_D = -C_M \omega_z^2 \operatorname{sgn}(\omega_z) \tag{9}$$

where  $|V_C|$  is the linear velocity magnitude of the body in the body-fixed frame and is defined as  $|V_c| = \sqrt{V_{c_x}^2 + V_{c_y}^2}, \; S_A$ is the wetted surface area for the robot,  $C_D$  is the drag force coefficient,  $C_L$  is the lift force coefficient,  $C_M$  is the drag moment coefficient, and  $sgn(\cdot)$  is the signum function.

# C. Hydrodynamic Forces from Rowing Pectoral Fins

As shown in Fig. 1(b), we consider the pectoral fins to be rectangular with span length  $S_p$ , and chord length  $D_p$ , and assume they perform pure rowing motion. To evaluate its hydrodynamic forces we adopt the procedure proposed in [28]. Furthermore, we illustrate the force calculations using only the right pectoral fin, since they can be trivially extended to the left pectoral fin.

The hydrodynamic forces on the pectoral fin have both spanwise and normal components. However, the fins are considered to have pure rowing motion which implies that the span-wise force that arises from friction is very small and can thus be neglected [29]. Using blade theory, we can then calculate the differential normal force  $dF_n(s,t)$  on each blade element dson the pectoral fin at time t as

$$\mathrm{d}F_{nR}(s,t) = \frac{1}{2}C_n(\varphi(s,t))\rho D_p |\vec{v}_p(s,t)|^2 \mathrm{d}s \qquad (10)$$

where  $C_n(\varphi(s,t)) = \lambda \sin \varphi$  is the normal force coefficient, which depends of the angle of attack of each arbitrary blade,  $\varphi(s,t)$ , and  $\lambda$  is a parameter that can be evaluated empirically through experiments. The velocity and acceleration at the point s along the fin are then given by

$$v_{p_R}(s,t) = s\dot{\gamma}_R \hat{n}^R \tag{11}$$

$$a_R(s,t) = s\ddot{\gamma}_R \hat{n}^R - s\dot{\gamma}_R^2 \hat{m}^R \tag{12}$$

where  $\dot{\gamma}_R$  and  $\ddot{\gamma}_R$  indicate the first and second time derivatives of  $\gamma_R$ , respectively.  $\hat{m}^R$  and  $\hat{n}^R$  are the unit vectors that define the coordinate system that is attached to the pectoral fin. The relationship between these unit vectors and the robotic fish body-fixed coordinates is given by

$$\hat{m}^R = \cos \gamma_R \hat{x} - \sin \gamma_R \hat{y} \tag{13}$$

$$\hat{n}^R = -\sin\gamma_R \hat{x} - \cos\gamma_R \hat{y} \tag{14}$$

The total hydrodynamic force acting on each pectoral fin is calculated by integrating the force density along the span length of the fin such that

$$F_{n_R}(t) = \int_0^{S_p} dF_{n_R}(s, t)$$
 (15)

The total force acting on the right fin is determined by

$$\vec{F}_R = F_{n_R} \, \hat{n}^R - \vec{F}_{A_0 R} = m_p a_R(s, t) \big|_{s = \frac{S_P}{2}}$$
 (16)

where  $\vec{F}_{A_0}$  represents the force applied by the rigid pectoral fin on the servo joint, and  $m_p$  is the effective mass of the rigid fin (the fin mass  $m_{pf}$  and the added mass, where the added mass is calculated based on a rigid plate moving in water [30]).

The moment of the fin relative to its pivot point  $(A_{0R})$  is given by

$$\vec{M}_{n_R} = \int_0^{S_p} s\hat{m}_R \times dF_{n_R} \tag{17}$$

Finally, the force and moment exerted on the robotic fish body by the right pectoral fin is given by

$$f_{h_x R} = \langle \vec{F}_{A_0 R}, \hat{x} \rangle$$
 (18)

$$f_{h_y R} = \langle \vec{F}_{A_0 R}, \hat{y} \rangle$$
 (19)

$$\tau_{h_z R} = C_p \hat{y} \times \vec{F}_{A_0} = C_p f_{h_x R} \hat{k} \tag{20}$$

For a more comprehensive derivation of the hydrodynamic forces, we refer the reader to [28]. By letting  $\ddot{\gamma}_R = \dot{\omega}_R$ ,  $\ddot{\gamma}_L = \dot{\omega}_L, \ u_1 = \dot{\omega}_R$  and  $u_2 = \dot{\omega}_L$ , and by considering the kinematic equations of the robotic fish, the dynamic model can be summarized as follows:

$$\begin{bmatrix} \dot{X} \\ \dot{Y} \\ \dot{V} \\ \dot{V} \\ \dot{V}_{c_x} \\ \dot{V}_{c_y} \\ \dot{\omega}_z \\ \dot{\gamma}_L \\ \dot{\omega}_R \end{bmatrix} = \begin{bmatrix} V_{c_x} \cos \psi - V_{c_y} \sin \psi \\ V_{c_x} \sin \psi + V_{c_y} \cos \psi \\ \omega_z \\ f_1(V_{c_x}, V_{c_y}, \omega_z) + \frac{f_{hx}}{m_1} \\ f_2(V_{c_x}, V_{c_y}, \omega_z) + \frac{f_{hy}}{m_2} \\ f_3(V_{c_x}, V_{c_y}, \omega_z) + \frac{\tau_{hz}}{J_3} \\ \omega_L \\ \omega_R \\ u_1 \\ u_2 \end{bmatrix}$$
(21)

with

$$f_{1}(V_{c_{x}}, V_{c_{y}}, \omega_{z}) = \frac{m_{2}}{m_{1}} V_{c_{y}} \omega_{z} - \frac{c_{1}}{m_{1}} V_{c_{x}} \sqrt{V_{c_{x}}^{2} + V_{c_{y}}^{2}} + \frac{c_{2}}{m_{1}} V_{c_{y}} \sqrt{V_{c_{x}}^{2} + V_{c_{y}}^{2}} \arctan(\frac{V_{c_{y}}}{V_{c_{x}}})$$

$$f_{2}(V_{c_{x}}, V_{c_{y}}, \omega_{z}) = -\frac{m_{1}}{m_{2}} V_{c_{x}} \omega_{z} - \frac{c_{1}}{m_{2}} V_{c_{y}} \sqrt{V_{c_{x}}^{2} + V_{c_{y}}^{2}}$$

$$V_{c_{x}} = \frac{c_{1}}{m_{2}} V_{c_{y}} \sqrt{V_{c_{x}}^{2} + V_{c_{y}}^{2}}$$
(23)

$$f_2(V_{c_x}, V_{c_y}, \omega_z) = -\frac{m_1}{m_2} V_{c_x} \omega_z - \frac{c_1}{m_2} V_{c_y} \sqrt{V_{c_x}^2 + V_{c_y}^2} - \frac{c_2}{m_2} V_{c_x} \sqrt{V_{c_x}^2 + V_{c_y}^2} \arctan(\frac{V_{c_y}}{V_{c_x}})$$
(23)

$$f_3(V_{c_x}, V_{c_y}, \omega_z) = \frac{(m_1 - m_2)}{J_3} V_{c_x} V_{c_y} - c_4 \omega_z^2 \operatorname{sgn}(\omega_z)$$
 (24)

where  $m_1=m_b-m_{a_x},\ m_2=m_b-m_{a_y},\ J_3=J_{bz}-J_{a_z},$   $c_1=\frac{1}{2}\rho SC_D,\ c_2=\frac{1}{2}\rho SC_L,\ c_4=\frac{1}{(J_3)}C_M$  . Note that  $f_{h_x}=f_{h_xR}+f_{h_xL},\ f_{h_y}=f_{h_yR}+f_{h_yL}$  and  $\tau_{hz}=\tau_{hzR}+\tau_{hzL}.$ 

# III. DUAL-LOOP FIN CONTROL SCHEME

#### A. Velocity Tracking Problem

The velocity tracking problem involves controlling the robot to track desired body-fixed velocity trajectories that are parameterized in time t. Given the underactuated nature and

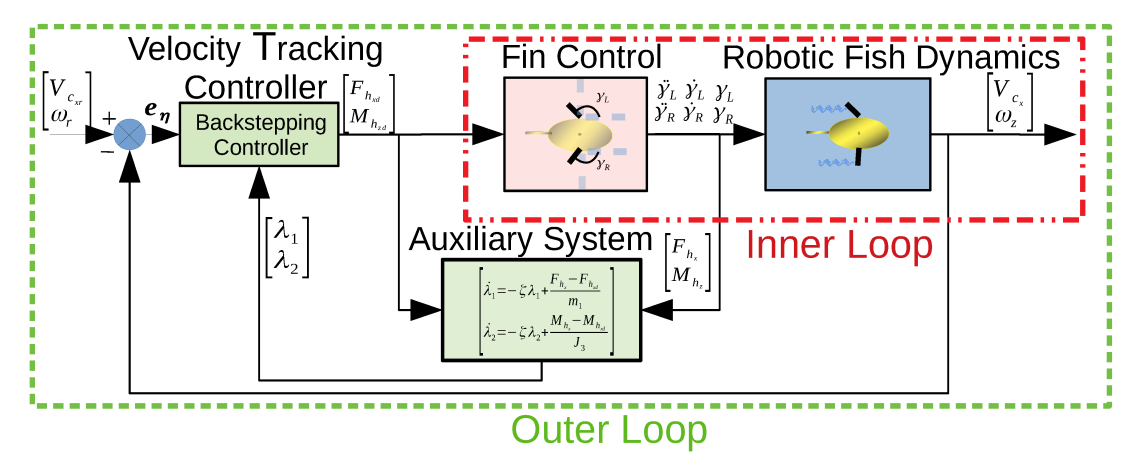


Fig. 2: Illustration of the proposed dual-loop pectoral fin-actuated robotic fish control scheme. The green dashed line encompasses the outer loop velocity tracking controller, while the inner red dotted and dashed line encompasses the fin movement planning and control algorithm.

input coupling of the robotic fish, tracking three velocities is challenging [31]; since the main focus of this work is in fin control we only consider tracking of the surge and angular velocity and leave the former for future work. Let the velocity tracking error at time t be given by

$$e_{\eta} = \begin{bmatrix} e_v \\ e_{\omega} \end{bmatrix} = \begin{bmatrix} V_{c_x} - V_{c_{xr}}(t) \\ \omega_z - \omega_r(t) \end{bmatrix}$$
 (25)

For brevity we drop the time-dependence for the remainder of the paper. By formulating the tracking problem in terms of the error state, the control objective becomes a stabilization problem, where the task is to find suitable control laws for  $u_1$ ,  $u_2$  such that for an arbitrary initial error, the states  $(e_v,e_\omega)$  of system (25) can be held near the origin (0,0).

# B. Velocity Tracking Control Algorithm

To achieve velocity tracking, a dual loop control structure is proposed. The outer loop is composed of a backstepping controller that determines the thrust and moment needed such that  $e_n \to 0$ . In particular, with sampling time  $t_s$ , the robotic fish and auxiliary system states are sampled. The robot's velocities are compared to the reference velocities  $V_{c_{xx}}$  and  $\omega_r$  and the tracking error  $e_{oldsymbol{\eta}}$  is then calculated. The error  $e_{\eta}$  is used by the outer loop controller (i.e the backstepping controller) to determine the thrust  $F_{h_xd}$  and moment  $M_{h_zd}$ needed to drive  $e_n$  to the origin. On the other hand, the inner loop is composed of a pectoral fin controller that determines the inputs  $u_1$  and  $u_2$  such that the pectoral fins generate a thrust  $F_{h_x}$  and moment  $M_{h_z}$  that are close to the desired values  $F_{h_xd}$  and  $M_{h_zd}$ . The robotic fish dynamics are then propagated using  $u_1$  and  $u_2$ , and the difference between the generated and desired thrust is captured by the states of an auxiliary system which is used along with the backstepping controller to guarantee closed-loop stability. At time  $t + t_s$  the process repeats. Fig. 2 illustrates the proposed method. A detailed overview of proposed control approach will be provided in the following sub-sections.

#### C. Velocity Tracking Control Synthesis

Backstepping control is a practical and systematic approach that provides stability guarantees, which makes it an attractive choice for velocity tracking. In this work, a backstepping-based controller is proposed to determine the thrust and moments necessary to drive the states  $(e_v, e_\omega)$  of the error system (25) to a neighborhood of the origin.

In order to successfully stabilize the error states to the origin and guarantee closed-loop stability, the backstepping controller must accommodate magnitude constraints on the thrust  $f_{h_x}$  and moments  $\tau_{h_z}$  that can be generated by the pectoral fins at a given time. In order to address this limitations, we adopt a similar scheme to that proposed in [31], [32].

Let  $F_{h_xd}$  and  $M_{h_zd}$  represent the nominal backstepping control inputs, and let  $F_{h_x}$  and  $M_{h_z}$  be the forces and moments that that can be practically implemented by the fins. Note that the  $F_{h_x}$  and  $M_{h_z}$  will be determined by the inner loop fin controller. To analyze the influence of the input difference, the following auxiliary system is chosen

$$\dot{\lambda}_1 = -\zeta_1 \lambda_1 + \frac{F_{h_x} - F_{h_x d}}{m_1}$$

$$\dot{\lambda}_2 = -\zeta_2 \lambda_2 + \frac{M_{h_z} - M_{h_z d}}{J_3}$$
(26a)

$$\dot{\lambda}_2 = -\zeta_2 \lambda_2 + \frac{M_{h_z} - M_{h_z d}}{J_2}$$
 (26b)

The auxiliary system composed of the variables  $\lambda_1$  and  $\lambda_2$  defined above represents the filtered effect of the nonachievable portion of the control inputs. In other words, they represent the additional tracking error that arises because of the mismatch between the nominal and implementable forces

To stabilize the  $(e_v,\ e_\omega)$  subsystem while also considering the difference in inputs, the following candidate Lyapunov

function is proposed

$$V_1 = \frac{1}{2}\bar{e}_v^2 + \frac{1}{2}\bar{e}_\omega^2 = \frac{1}{2}(e_v - \lambda_1)^2 + \frac{1}{2}(e_\omega - \lambda_2)^2$$
 (27)

where  $\bar{e}_v$  and  $\bar{e}_\omega$  are the modified tracking errors. The time derivative of Eq. (27) is given by

$$\dot{V}_{1} = \bar{e}_{v}\dot{\bar{e}}_{v} + \bar{e}_{\omega}\dot{\bar{e}}_{\omega} 
= \bar{e}_{v}(f_{1}(V_{c_{x}}, V_{c_{y}}, \omega_{z}) - \dot{V}_{c_{xr}} + \frac{F_{h_{x}d}}{m_{1}} + \zeta_{1}\lambda_{1}) + 
\bar{e}_{\omega}(f_{3}(V_{c_{x}}, V_{c_{y}}, \omega_{z}) - \dot{\omega}_{r} + \frac{M_{h_{z}d}}{J_{2}} + \zeta_{2}\lambda_{2})$$
(28)

Let  $F_{h_{xd}}$  and  $M_{h_{zd}}$  be given by

$$F_{h_{xd}} = m_1(-f_1(V_{c_x}, V_{c_y}, \omega_z) + \dot{V}_{c_{xr}} - \zeta_1 \lambda_1 - K_{\bar{e}_v} \bar{e}_v) \quad (29a)$$

$$M_{h_z d} = J_3(-f_3(V_{c_x}, V_{c_y}, \omega_z) + \dot{\omega}_r - \zeta_2 \lambda_2 - K_{\bar{e}_\omega} \bar{e}_\omega)$$
 (29b)

such that (28) becomes

$$\dot{V}_1 = -K_{\bar{e}_v}\bar{e}_v^2 - K_{\bar{e}_\omega}\bar{e}_\omega^2 \tag{30}$$

If  $K_{\bar{e}_v}>0$  and  $K_{\bar{e}_\omega}>0$ , then  $\dot{V}_1<0$  except when  $\bar{e}_v=\bar{e}_\omega=0$  implying the convergence of  $(\bar{e}_v,\bar{e}_\omega)$  to zero as time approaches infinity. Given that  $0\leq \bar{V}_1(t)\leq \bar{V}_1(0)$ , one can conclude that  $(\bar{e}_v,\bar{e}_\omega)$  belongs to  $\mathcal{L}_2$ , which implies that even when the desired force and moment are not implemented, the quantities  $\bar{e}_v$  and  $\bar{e}_\omega$  do not diverge. While the convergence for the modified tracking errors  $\bar{e}_v$  and  $\bar{e}_\omega$  is guaranteed, that of the actual velocity tracking errors  $e_v$  and  $e_\omega$  is not, as the latter may actually increase during periods when the force and moment limitations are in effect and the desired values cannot be implemented (i.e.  $F_{h_x}\neq F_{h_xd}$  and/or  $M_{h_z}\neq M_{h_zd}$ ). On the other hand, when the control signal limitations are not in effect, (i.e.  $F_{h_x}=F_{h_xd}$  and  $M_{h_z}=M_{h_zd}$ ),  $\lambda_1$  and  $\lambda_2$  approach zero, and  $(\bar{e}_v,\bar{e}_\omega)$  converges towards  $(e_v,e_\omega)$  and the velocity error can be stabilized.

From Eq. (20) and Eqs. (29a)-(29b), the desired left and right pectoral fin forces can be determined as

$$f_{h_x dL} = \frac{J_3}{2C_p} (-f_3(V_{c_x}, V_{c_y}, \omega_z) + \dot{\omega}_r + \zeta_2 \lambda_2 - K_{\bar{e}_{\omega}} \bar{e}_{\omega}) - \frac{m_1}{2} (-f_1(V_{c_x}, V_{c_y}, \omega_z) + \dot{V}_{c_{xr}} - \zeta_1 \lambda_1 - K_{\bar{e}_v} \bar{e}_v)$$

$$J_3 \left( -f_1(V_{c_x}, V_{c_y}, \omega_z) + \dot{V}_{c_{xr}} - \zeta_1 \lambda_1 - K_{\bar{e}_v} \bar{e}_v \right)$$

$$f_{h_x dR} = \frac{J_3}{2C_p} \left( -f_3(V_{c_x}, V_{c_y}, \omega_z) + \dot{\omega}_r + \zeta_2 \lambda_2 - K_{\bar{e}_{\bar{\omega}}} \bar{e}_{\bar{\omega}} \right) + \frac{m_1}{2} \left( -f_1(V_{c_x}, V_{c_y}, \omega_z) + \dot{V}_{c_{xr}} - \zeta_1 \lambda_1 - K_{\bar{e}_v} \bar{e}_v \right)$$
(32)

#### D. Pectoral Fin Control Algorithm

The goal of the pectoral fin control algorithm is to determine the inputs  $u_1$  and  $u_2$  such that pectoral fin movement generates forces that track the desired forces  $f_{h_x dL}$  and  $f_{h_x dR}$ .

To achieve this goal, we propose a model-predictive planning algorithm to determine an angular acceleration trajectory for each fin that accommodates the feasibility of the fin movement while producing a thrust that is close to the desired value for a given interval of time  $T_p$ , where  $T_p = t_s$ .

The general procedure to determine the angular trajectory is as follows:  $T_P$  is discretized into multiple evenly spaced sub-intervals. For the first sub-interval, a fixed number of

B different possible (constant) fin acceleration choices are generated by randomly sampling a distribution (the design of which will be discussed later), and their corresponding angular velocities, positions and force trajectories within the said subinterval are calculated based on a constant-acceleration model. For the next sub-interval, for each choice previously generated, a new set of B choices for the acceleration are generated and once again the fins'angular velocities, positions and force trajectories within the sub-interval are calculated for all choices. The process repeats until the total number of sub-intervals is reached. In this manner the number of choices per sub-interval increases exponentially with the sub-interval stage. Fig. 3 depicts an example of the general idea, where different possible acceleration, velocity and position trajectories generated for a planning interval  $T_P$  are shown. The assemblage of individual angular accelerations values (and corresponding position and velocities) from each interval is considered a plausible angular trajectory for the period  $T_p$ . Each possible angular trajectory is assigned a cost that is dependent on the difference between its corresponding generated force trajectory and the desired value. The trajectory that yields the lowest cost is selected as the solution. To elaborate on the control algorithm in detail, we utilize the right fin as an example; however, the same approach can be trivially extended to the left pectoral fin.

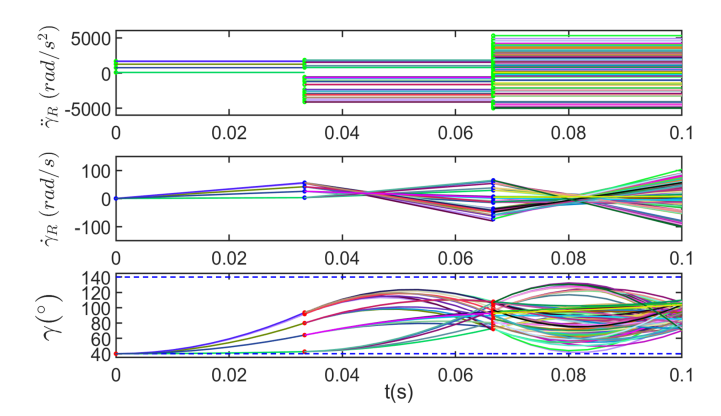


Fig. 3: Example of different possible fin acceleration, velocity and position trajectories generated within a planning interval  $T_P$  that is divided into three sub-intervals.

The outer loop control inputs are updated every  $t_s$  seconds and new  $f_{h_x dL}$  and  $f_{h_x dR}$  forces are calculated. For the duration of  $t_s$ , the desired forces remain constant and become the tracking reference for the fin control algorithm. Note that  $T_p = t_s$ . Let  $T_P$  be discretized into  $n_0$  evenly spaced subintervals of length  $\Delta t$  and let  $\ddot{\gamma}_{Ri}$  be constant throughout the ith sub-interval, where  $i=1,\cdots,n_0$ . At a given ith subinterval there will be  $B^i$  different choices for  $\ddot{\gamma}_R$ , such that for a given period  $T_P$  there area a total of  $B^{n_0}$  possible choices of (piecewise constant) acceleration trajectories.

For a given choice of angular accelerations up to the beginning of the ith sub-interval, the following elaborates on the procedure for the related computation:

# 1. Determine allowed range for $\ddot{\gamma}_R$ : Given that the pec-

toral fins position  $\gamma_R$  is physically limited, the allowed angular velocities  $\dot{\gamma}_R$  and angular acceleration  $\ddot{\gamma}_R$  are constrained to lie within a range dependent on the current fin's position and velocity. Since  $\ddot{\gamma}_R$  is constant throughout each sub-interval, using the standard constant acceleration model the allowed  $\ddot{\gamma}_R$ within  $\Delta t$  can determined as follows

$$\ddot{\gamma}_{R(max)i} = \frac{2(\gamma_{Rmax} - \gamma_{R0}^{(i)} - \dot{\gamma}_{R0}^{(i)} \Delta t)}{(\Delta t)^2}$$
(33a)

$$\ddot{\gamma}_{R(min)i} = \frac{2(\gamma_{Rmin} - \gamma_{R0}^{(i)} - \dot{\gamma}_{R0}^{(i)} \Delta t)}{(\Delta t)^2}$$
 (33b)

where  $\gamma_{Rmax}$  and  $\gamma_{Rmin}$  denote the maximum and minimum allowed fin position, respectively, while  $\gamma_{R0}^{(i)}$  and  $\dot{\gamma}_{R0}^{(i)}$  denote the value of  $\gamma_R$  and  $\dot{\gamma}_R$  at the beginning of the *i*th sub-interval, respectively.

**2. Calculate desired**  $\ddot{\gamma}_{Rd}$ : Given  $f_{h_x dR}$ , a desired  $\ddot{\gamma}_{Rd}$  is calculated from Eq. (18) as follows

$$\ddot{\gamma}_{Rdi} = -\frac{\lambda \rho D_p S_p^2 (\dot{\gamma}_{R0}^{(i)})^2 \operatorname{sgn}(\dot{\gamma}_{R0}^{(i)})}{3m_p} - \frac{(\dot{\gamma}_{R0}^{(i)})^2 \cos \gamma_{R0}^{(i)}}{\sin \gamma_{R0}^{(i)}} + \frac{2f_{h_x Rd}}{S_p m_p \sin \gamma_{R0}^{(i)}}$$
(34)

3. Generate the sampling distribution and sample BThe B different  $\ddot{\gamma}_R$  values are sampled from a distribution which is generated by dividing the allowable  $\ddot{\gamma}_{Ri}$ range into N evenly spaced discrete values. Each possible nth value is assigned a normalized weight  $W_n$  determined by the following:

$$W_n = \frac{e^{-d_n}}{\sum_{n=1}^N e^{-d_n}} \tag{35}$$

where  $n=1,\cdots N$ , and  $d_n=\sqrt{(\ddot{\gamma}_{Ri}^{(n)}-\ddot{\gamma}_{Rd})^2}$  is the Euclidean distance between the nth  $\ddot{\gamma}_{Ri}$  value and the desired  $\ddot{\gamma}_{Rdi}$ . Note  $\Sigma_{n=1}^{N}W_{n}=1$ .

To sample from this distribution, generate P "particles", where each "particle" is representative of each discrete value of  $\ddot{\gamma}_{Ri}$ . The number of particles generated for a particular discrete value of  $\ddot{\gamma}_{Ri}$  is given by

$$P_n = W_n P \tag{36}$$

Note that  $P_n$  must be rounded to the nearest integer and that  $\sum_{n=1}^{N} P_n = P$ . Fig. 4 illustrates an example of the weights calculated for a given range of  $\ddot{\gamma}_{Ri}$ . Finally, B "particles" are uniformly sampled from the whole set of P particles, which results in random choices of  $\ddot{\gamma}_{Ri}$  with preference towards values closer to  $\ddot{\gamma}_{Rd}$ .

**4.** Calculate  $\gamma_{Ri}$  and  $\dot{\gamma}_{Ri}$ : For a given  $\ddot{\gamma}_{Ri}$ , the resultant  $\dot{\gamma}_R^{(i)}$  and  $\gamma_R^{(i)}$  trajectories can be obtained from the constant acceleration model as follows

$$\gamma_R^{(i)}(t_i, t_{i+1}) = \gamma_{R0} + \dot{\gamma}_{R0}^{(i)}t + \frac{1}{2}\ddot{\gamma}_{Ri}t^2$$
 (37a)

$$\dot{\gamma}_R^{(i)}(t_i, t_{i+1}) = \dot{\gamma}_{R0}^{(i)} + \ddot{\gamma}_{Ri}t \tag{37b}$$

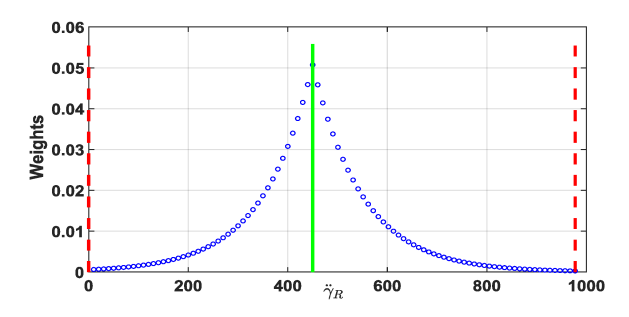


Fig. 4: Example of weights for each value of  $\ddot{\gamma}_{Ri}$  within a given allowed range. The vertical dotted red lines indicate the maximum and minimum values allowed for  $\ddot{\gamma}_{Ri}$  in the ith interval, while the green solid line represents the desired value.

where  $t \in [t_i, t_{i+1}]$ .

5. Determine the force  $f_{h_xR}^{(i)}$  for a given  $\ddot{\gamma}_{Ri}$ : From Eq. (18), the force generated by the fin in the ith interval is

$$f_{h_xR}^{(i)}(t_i, t_{i+1}) = \frac{1}{6} \lambda \rho D_p S_p^3 (\dot{\gamma}_R^{(i)})^2 \sin \gamma_R^{(i)} \operatorname{sgn}(\dot{\gamma}_R^{(i)}) - m_p \left(-\frac{S_p}{2} \ddot{\gamma}_R^{(i)} \sin \gamma_R^{(i)} - \frac{S_p}{2} (\dot{\gamma}_R^{(i)})^2 \cos \gamma_R^{(i)}\right)$$
(38)

**6. Calculate cost for each**  $\ddot{\gamma}_{Ri}$ : A cost is assigned to each generated acceleration choice within the ith sub-interval. The cost function is given by

$$K^{i} = \left(\int_{t_{*}}^{t_{i+1}} f_{h_{x}R}^{(i)}(\tau) - \int_{t_{*}}^{t_{i+1}} f_{h_{x}Rd}\right)^{2} d\tau \qquad (39)$$

7. Determine best  $\ddot{\gamma}_R$  trajectory among the  $B^{n_0}$  candidates:

$$\min_{\tilde{\gamma}_R(\cdot)} \sum_{p=1}^{n_0} K^i \tag{40}$$

Note that in steps 1-5 sets of possible accelerations for each interval are generated, while in the steps 6-7 the best candidate is determined. Furthermore, by sampling from the skewed distribution presented in step 3, we take into consideration the ideal  $\ddot{\gamma}_{Rd}$ , which allows us to make an educated guess as to what possible  $\ddot{\gamma}_R$  should be generated in order to find a good solution. Finally, since the algorithm considers the angular position constraints, a plausible  $\ddot{\gamma}_R$  trajectory is always

Once the best  $\ddot{\gamma}_R$  and  $\ddot{\gamma}_L$  are selected, the total hydrodynamic force  $F_{h_x}$  and moment  $M_{h_z}$  that will be exerted by the robotic fish can be calculated, and the auxiliary system states can be updated.

#### IV. SIMULATION

To evaluate the effectiveness of the designed controller, simulations were carried out using MATLAB. The robotic fish parameters used for simulation are listed in Tab. I.

Furthermore, the backstepping controller and planning algorithm parameters were chosen as follows:

TABLE I: PARAMETERS OF THE ROBOTIC FISH [9].

| Parameter | Value   | Parameter   | Value                 |
|-----------|---|-------------|-----------------------|
| $m_b$     | 0.295 kg  | $m_{ax}$    | -0.095 kg             |
| $m_{ay}$  | -0.1794 kg  | $\rho$      | $1000 \text{ kg/m}^3$ |
| $J_{bz}$  | $2.66 \times 10^{-3} \text{ kg} \cdot \text{m}^2$ | $C_L$       | 4.86                  |
| $J_{az}$  | $-2.7 \times 10^{-5} \text{ kg/m}^2$              | $C_D$       | 0.42                  |
| $C_M$     | $7.6 \times 10^{-4} \text{ kg/m}^2$               | $S_A$       | 0.0325 m              |
| $S_p$     | 0.043 m   | $C_p$       | 0.025 m               |
| $m_p$     | 0.0194 m  | $\hat{D_p}$ | 0.025                 |

$$\begin{array}{lll} K_{\bar{e}_v} = 1.8 & K_{\bar{e}_\omega} = 1.4 \\ \zeta_1 = 1.3 & \zeta_2 = 1.9 \\ \gamma_{Rmin} = \gamma_{Lmin} = 40^\circ & \gamma_{Rmax} = \gamma_{Lmax} = 140^\circ \\ t_s = 0.1 \text{ s} & T_P = 0.1 \text{ s} \\ n_0 = 2 & B = 15 \\ N = 40 & P = 500 \end{array}$$

where the variable  $t_s$  is the sampling interval which pertains to the amount of time between an update to the desired force and moment values,  $F_{h_x d}$  and  $M_{h_z d}$ . The backstepping controller parameters were chosen such that under the right values the velocity error system was stabilized to a neighborhood of the origin. We found that  $K_{\bar{e}_v}$  and  $K_{\bar{e}_\omega}$  regulate the balance between the convergence rate of the  $e_v$  and  $e_\omega$  error, respectively, while varying  $\zeta_1$  and  $\zeta_2$  regulates the convergence rate of the control-deviation errors  $\lambda_1$  and  $\lambda_2$ , respectively. The randomized model-predictive planning scheme parameters,  $n_0$ , B, N and P, were chosen as to balance the trade-off between computational effort and performance.

To demonstrate the effectiveness of the proposed approach, simulations were carried out to compare its performance with an alternative approach, where NMPC is used as the inner loop fin controller. The cost function Eq. (39) was adopted to the NMPC algorithm, and the NMPC parameters were chosen as follows:

Prediction Horizon= 0.1 Control Intervals = 30 
$$Q=5000$$
  $t_s=0.1$  s

where the weighting matrix Q was chosen to heavily penalize the deviation from the desired force and the force being generated, and the prediction horizon was chosen as the length of the sampling time  $t_s$ . The following reference velocity trajectory, with abrupt changes, was considered in simulations

$$\begin{cases} V_{c_{x_r}} = 0.02 \text{ m/s}, \ \omega_r = 0.02 \text{ rad/s} & t < 1 \\ V_{c_{x_r}} = 0.02 \text{ m/s}, \ \omega_r = -0.2 \text{ rad/s} & 1 \leq t < 2 \\ V_{c_{x_r}} = 0.02 \text{ m/s}, \ \omega_r = 0.2 \text{ rad/s} & 2 \leq t < 3 \\ V_{c_{x_r}} = 0.01 \text{ m/s}, \ \omega_r = 0.1 \text{ rad/s} & 3 \leq t < 4 \\ V_{c_{x_r}} = 0.01 \text{ m/s}, \ \omega_r = 0 \text{ rad/s} & 4 \leq t \end{cases}$$

In Fig. 5 the desired and the closed-loop velocity trajectories of the robotic fish are depicted for the proposed method and the alternative NMPC scheme, while Fig. 6 illustrates the fin positions over time for each scheme. From Fig. 5 one can see that the proposed approach allows the robot to respond to the sudden changes of the desired velocities. In particular,

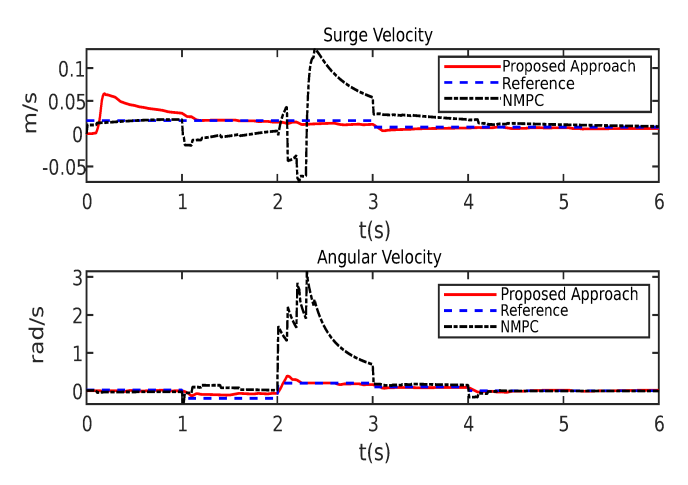


Fig. 5: Simulation: velocity-tracking trajectories results for the proposed scheme and the alternative scheme with NMPC for the inner loop controller.

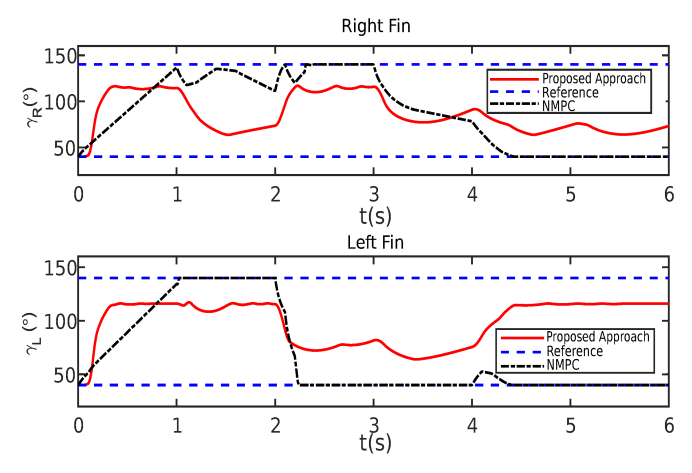


Fig. 6: Simulation: fin position trajectories resulting from the proposed scheme and the alternative scheme with NMPC for the inner loop controller. The dashed blue lines depict the fin's position constraints.

aside from the initial overshoot, the robot was able to keep approaching the desired surge velocity while tracking the quickly-varying reference angular trajectory. Furthermore, the surge and angular velocity cumulative tracking errors for the proposed approach is 0.0006 and 0.0188, respectively. On the other hand, for the alternative NMPC scheme the cumulative tracking errors are 0.0053 and 2.2431 for the surge and angular velocity, respectively. From the tracking error cost one can see that although the NMPC approach is able to handle the fin range constraints, its tracking performance is inferior when compared to the proposed approach. Finally, from Fig. 6, one can note that for both approaches the fin's positions constraints are not violated, however, unlike the NMPC approach the proposed approach does not saturate the fin's position.

#### V. CONCLUSION

In this work, a systematic approach for maneuvering control of a pectoral-fin actuated robotic fish was proposed. Specifically, we proposed a dual loop control scheme consisting of an outer-loop backstepping controller and an inner loop fin movement-planning algorithm. In particular, the outer loop backstepping-controller finds the thrust and moment required to stabilize the velocity tracking error, while the inner loop plans the motion of the fin for a given time-interval to produce a thrust and a moment close to their desired values by utilizing a randomized sampling algorithm. To illustrate the challenges in control, the velocity tracking problem with abrupt velocity changes for a robotic fish was considered. Simulation results showed the effectiveness of the proposed scheme and and its superiority over an alternative employing an NMPC in the inner loop.

For future work, the proposed scheme will be optimized to accommodate the trade-off between performance and computational efficiency. Furthermore, the algorithm will be extended to other tasks such as trajectory tracking, which requires addressing the challenge of under-actuation and input coupling. Finally, experiments will be implemented on a robotic fish prototype to verify the effectiveness of the proposed approach.

#### REFERENCES

- [1] X. Tan, "Autonomous robotic fish as mobile sensor platforms: Challenges and potential solutions," pp. 31–40, 2007.
- [2] F. Zhang, O. Ennasr, E. Litchman, and X. Tan, "Autonomous sampling of water columns using gliding robotic fish: Algorithms and harmfulalgae-sampling experiments," *IEEE Systems Journal*, vol. 10, no. 3, pp. 1271–1281, 2015.
- [3] S. Marras and M. Porfiri, "Fish and robots swimming together: attraction towards the robot demands biomimetic locomotion," *Journal of The Royal Society Interface*, vol. 9, no. 73, pp. 1856–1868, 2012.
- [4] M. S. Triantafyllou and G. S. Triantafyllou, "An efficient swimming machine," *Scientific American*, vol. 272, no. 3, pp. 64–70, 1995.
- [5] P. Kodati, J. Hinkle, A. Winn, and X. Deng, "Microautonomous robotic ostraciiform (MARCO): Hydrodynamics, design, and fabrication," *IEEE Transactions on Robotics*, vol. 24, no. 1, pp. 105–117, 2008.
- [6] G. V. Lauder, P. G. Madden, R. Mittal, H. Dong, and M. Bozkurttas, "Locomotion with flexible propulsors: I. Experimental analysis of pectoral fin swimming in sunfish," *Bioinspiration & Biomimetics*, vol. 1, no. 4, p. S25, 2006.
- [7] K. A. Morgansen, T. M. La Fond, and J. X. Zhang, "Agile maneuvering for fin-actuated underwater vehicles," in *Proceedings of the 2006 Sec*ond International Symposium on Communications, Control and Signal Processing. Citeseer, 2006.
- [8] K. Low and A. Willy, "Biomimetic motion planning of an undulating robotic fish fin," *Journal of Vibration and Control*, vol. 12, no. 12, pp. 1337–1359, 2006.
- [9] S. B. Behbahani, "Role of flexibility in robotic fish," Ph.D. dissertation, Michigan State University, 2016.
- [10] H. Wang, "Design and implementation of biomimetic robotic fish," Master's thesis, Concordia University, 2009.
- [11] S. Vogel, Life in moving fluids: the physical biology of flow, 1996.
- [12] P. Duraisamy, R. K. Sidharthan, and M. N. Santhanakrishnan, "Design, modeling, and control of biomimetic fish robot: A review," *Journal of Bionic Engineering*, vol. 16, no. 6, pp. 967–993, 2019.
- [13] P. E. Sitorus, Y. Y. Nazaruddin, E. Leksono, and A. Budiyono, "Design and implementation of paired pectoral fins locomotion of labriform fish applied to a fish robot," *Journal of Bionic Engineering*, vol. 6, no. 1, pp. 37–45, 2009.

- [14] Z. Ye, P. Hou, and Z. Chen, "2D maneuverable robotic fish propelled by multiple ionic polymer–metal composite artificial fins," *International Journal of Intelligent Robotics and Applications*, vol. 1, no. 2, pp. 195–208, 2017.
- [15] N. Kato, "Locomotion by mechanical pectoral fins," *Journal of Marine Science and Technology*, vol. 3, no. 3, pp. 113–121, 1998.
- [16] D. Lachat, A. Crespi, and A. J. Ijspeert, "Boxybot: a swimming and crawling fish robot controlled by a central pattern generator," in *The First IEEE/RAS-EMBS International Conference on Biomedical Robotics and Biomechatronics*, 2006. BioRob 2006. IEEE, 2006, pp. 643–648.
- [17] X. Deng and S. Avadhanula, "Biomimetic micro underwater vehicle with oscillating fin propulsion: System design and force measurement," in Proceedings of the 2005 IEEE International Conference on Robotics and Automation. IEEE, 2005, pp. 3312–3317.
- [18] K. A. Morgansen, B. I. Triplett, and D. J. Klein, "Geometric methods for modeling and control of free-swimming fin-actuated underwater vehicles," *IEEE Transactions on Robotics*, vol. 23, no. 6, pp. 1184–1199, 2007.
- [19] M. Wang, J. Yu, and M. Tan, "Modeling neural control of robotic fish with pectoral fins using a CPG-based network," in *Proceedings of the* 48h IEEE Conference on Decision and Control (CDC) held jointly with 2009 28th Chinese Control Conference. IEEE, 2009, pp. 6502–6507.
- [20] M. Wang, J. Yu, M. Tan, and J. Zhang, "Design and implementation of a novel cpg-based locomotion controller for robotic dolphin," in 2010 8th World Congress on Intelligent Control and Automation. IEEE, 2010, pp. 1611–1616.
- [21] ——, "Multimodal swimming control of a robotic fish with pectoral fins using a CPG network," *Chinese Science Bulletin*, vol. 57, no. 10, pp. 1209–1216, 2012.
- [22] J. Yu, K. Wang, M. Tan, and J. Zhang, "Design and control of an embedded vision guided robotic fish with multiple control surfaces," *The Scientific World Journal*, vol. 2014, 2014.
- [23] S. Zhang, Y. Qian, P. Liao, F. Qin, and J. Yang, "Design and control of an agile robotic fish with integrative biomimetic mechanisms," *IEEE/ASME Transactions on Mechatronics*, vol. 21, no. 4, pp. 1846–1857, 2016.
- [24] M. Wang, J. Yu, and M. Tan, "CPG-based sensory feedback control for bio-inspired multimodal swimming," *International Journal of Advanced Robotic Systems*, vol. 11, no. 10, p. 170, 2014.
- [25] N. Kato, "Control performance in the horizontal plane of a fish robot with mechanical pectoral fins," *IEEE journal of oceanic engineering*, vol. 25, no. 1, pp. 121–129, 2000.
- [26] M. Aureli, V. Kopman, and M. Porfiri, "Free-locomotion of underwater vehicles actuated by ionic polymer metal composites," *IEEE/ASME* transactions on mechatronics, vol. 15, no. 4, pp. 603–614, 2009.
- [27] J. Wang, P. K. McKinley, and X. Tan, "Dynamic modeling of robotic fish with a base-actuated flexible tail," *Journal of dynamic systems, measurement, and control*, vol. 137, no. 1, 2015.
- [28] S. B. Behbahani and X. Tan, "Role of pectoral fin flexibility in robotic fish performance," *Journal of Nonlinear Science*, vol. 27, no. 4, pp. 1155– 1181, 2017.
- [29] E. G. Drucker, J. A. Walker, and M. W. Westneat, "Mechanics of pectoral fin swimming in fishes," *Fish Physiology*, vol. 23, pp. 369–423, 2005.
- [30] R. Dong, "Effective mass and damping of submerged structures," California Univ., Livermore (USA). Lawrence Livermore Lab., Tech. Rep., 1978
- [31] M. L. Castaño and X. Tan, "Backstepping control-based trajectory tracking for tail-actuated robotic fish," in 2019 IEEE/ASME International Conference on Advanced Intelligent Mechatronics (AIM). IEEE, 2019, pp. 839–844.
- [32] J. Farrell, M. Polycarpou, and M. Sharma, "Adaptive backstepping with magnitude, rate, and bandwidth constraints: Aircraft longitude control," in *Proceedings of the 2003 American Control Conference*, 2003., vol. 5. IEEE, 2003, pp. 3898–3904.